SAND99-0543C

Tutorial on Modeling and Control of Micro- and Nano-Manipulation, 1999 IEEE International Conference on Robotics and Automation, Detroit, May 11, 1999.

Parallel Assembly of LIGA Components

John T. Feddema, Todd R. Christenson
Sandia National Laboratories[1]
P.O. Box 5800, MS 1003
Albuquerque, NM 87185

Abstract

In this paper, a prototype robotic workcell for the parallel assembly of LIGA components is described. A Cartesian robot is used to press 386 and 485 micron diameter pins into a LIGA substrate and then place a 3-inch diameter wafer with LIGA gears onto the pins. Upward and downward looking microscopes are used to locate holes in the LIGA substrate, pins to be pressed in the holes, and gears to be placed on the pins. This vision system can locate parts within 3 microns, while the Cartesian manipulator can place the parts within 0.4 microns.

Introduction

When developing MEMS (Micro-ElectroMechanical Systems), there are three primary technologies: surface micromachined silicon, bulk micromachined silicon, and LIGA (Lithography Galvonoforming Abforming). All three technologies have their own advantages and disadvantages. For instance, the surface and bulk micromachined silicon technologies take advantage of the infrastructure and machinery developed for producing integrated circuits [1]. This infrastructure has been designed for massively parallel fabrication, where hundreds of identical copies of the same device are replicated on a single silicon wafer. On the downside, this same infrastructure limits the types and thickness of materials, and the design of these devices. Typically, the silicon-based materials are used. Also, the devices are typically designed to be planar, although pop-up three-dimensional structures have been demonstrated [2].

LIGA is an alternative technology, where the component sizes typically lie between conventionally machined components and surface micromachined silicon components [3][4]. The advantages of the LIGA approach are that the individual piece parts can be fabricated out of metals and plastics, and they are typically thicker than surface micromachined parts. Although the parts are typically limited to stepwise prismatic shapes, the parts can be assembled into complex, three-dimensional structures, which is a requirement for high aspect ratio precision micro-scaled components. Unfortunately, this assembly step is a time consuming, labor intensive process, which greatly limits the mass production of the LIGA devices.

In the past, many researchers have investigated the assembly of individual MEMS components with teleoperated robotic devices [5-7]. More recently, semi-automated assembly systems with vision and force feedback have been developed [8-12]. However, all of these systems only manipulate individual components. In the future, for LIGA to be more widely accepted as an analogous process to planar microfabrication, a means of batch manufacturing is needed [13][14]. Similar to the parallel fabrication process of silicon surface machined devices, LIGA-fabricated MEMS need to be fabricated and assembled using "standard" processes that are parallel in nature. In this paper, we investigate the assembly of parallel LIGA parts and the use of multiple cameras for visual feedback.

As an example, imagine building 100 LIGA-fabricated transmissions in parallel. For a geared transmission to be formed, multiple layers of LIGA gears would have to be bonded together and released onto pins (see Figure 1). Sandia National Laboratories has shown that it may be possible to do this by using diffusion bonding to adhere layers of LIGA parts [15]. The "standard" processes would consist of four steps: fabrication, assembly, diffusion bonding, and release. These steps would be repeated several

[1] Sandia is a multiprogram laboratory operated by Sandia Corporation, a Lockheed Martin Company, for the United States Department of Energy under contract DE-AC04-94AL85000.

times, each time adding a new layer of LIGA to the final assembly. The fabrication step is the standard LIGA process of developing a PMMA (polymethylmethacrylate) mold using X-ray lithography, electroplating the metal on the wafer, and removing the PMMA mold, thus leaving the LIGA layer on the wafer. The assembly step consists of aligning and mating two LIGA layers on two separate wafers. The diffusion-bonding step adheres the new layer of LIGA to a previous layer of LIGA. The release step chemically etches the thin sacrificial layer of the top wafer, thus releasing this LIGA layer. In this paper, we will discuss in detail only the assembly step. The details of the other two steps are still being actively pursued.

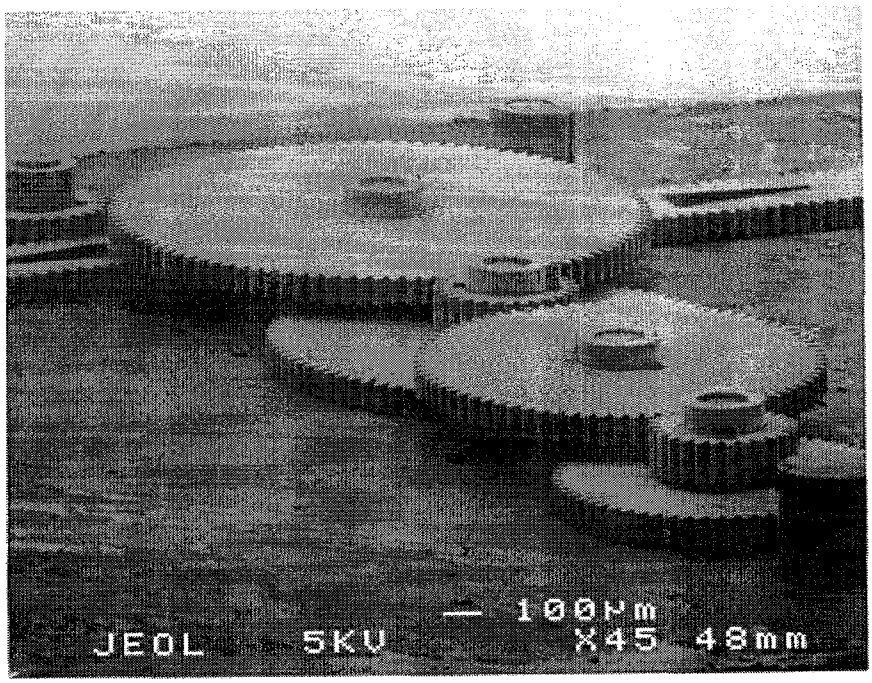

Figure 1. Geared transmission made of LIGA parts.

The next several sections describe our prototype workcell, a vision calibration routine, and the experimental results. Conclusions and suggestions for future work are given at the end of the paper.

Parallel Assembly Workcell

At Sandia National Laboratories, we have designed, fabricated, and tested a workcell that presses 386 and 485 micron diameter pins into a LIGA substrate and then places a 3-inch diameter wafer with LIGA gears on the pins. The workcell consists of 4 DOF (Degree of Freedom) AMTI (subsidiary of ESEC) Cartesian assembly system, two long working distance microscopes, a pin insertion tool, a wafer-handling vacuum chuck, and a wafer pallet. The AMTI robot has a repeatability of 0.4 microns in the x and y directions, 8 microns in the z direction, and 0.006 degrees in rotation about z. The downward looking microscope is mounted to the x,y,z stages of the robot, while the upward looking microscope is mounted next to the wafer pallet.

Figures 2 and 3 show the layout of our parallel assembly system. A pallet under the AMTI robot holds three 3-inch diameter silicon wafers. The wafer in the middle has a LIGA substrate bonded to it. This substrate contains 382 micron and 481 micron diameter holes. The wafer to the left contains 386 and 485 micron pins, which have been manually placed in clearance holes (392 and 492 microns). The wafer to the right is upside down and contains LIGA gears (with 394 and 496 clearance holes) still bonded to the plating material on the wafer. The robot first picks up the pins from the wafer on the left, press fits them into the

DISCLAIMER

wafer in the middle, and then places the wafer on the right onto the wafer in the middle such that the pins and gears align. The resulting wafer sandwich would then be taken to a chemical bath where the thin metal sacrificial layer on the top wafer would be removed, thus releasing the gears. The gears would then be free to rotate on the press-fit pins.

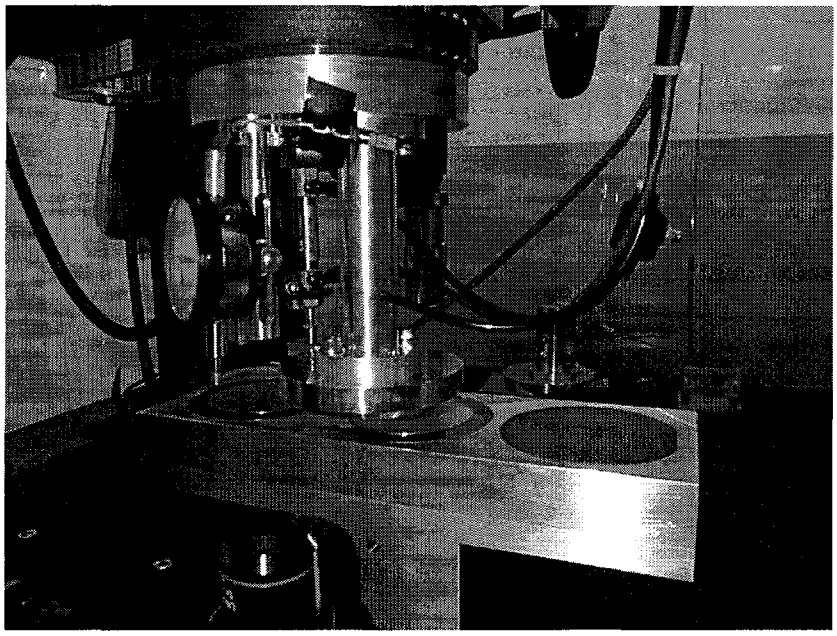

Figure 2. Parallel assembly lay-out used to insert pins and align wafers. The upward looking microscope is visible in the lower left of the picture.

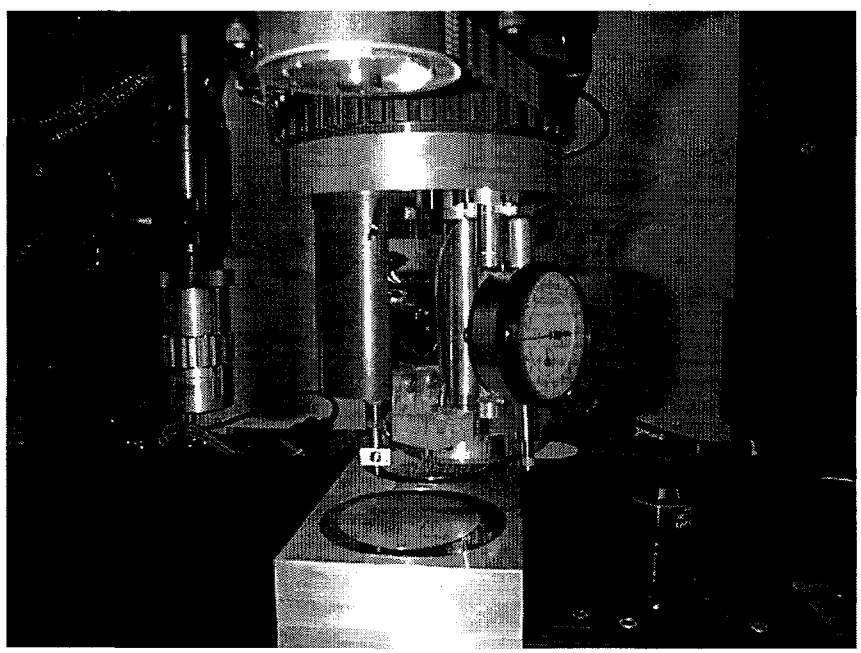

Figure 3. Perpendicular view of parallel assembly lay-out. Downward looking microscope is on the left side of the picture, and the upward looking microscope is on the right.

Three tools are mounted on the end of the AMTI robot. The first is a dial gage, which is used to align the surface of the pallet with the AMTI x,y plane. The second tool is a pin insertion tool, which contains a vacuum tip for picking up a pin and a vertical pneumatic actuator for pressing the pin to a specified force. The third tool is a vacuum chuck for picking up and placing the wafer of gears onto the wafer of inserted pins.

Vision System Calibration

Calibration of the vision system is key to the localization and alignment of the pins and gears. The exact locations of the pins, gears, pin insertion tool, and wafer-handling tool are not known *a priori*. Instead, we use the vision system to determine these locations.

A 3-inch diameter calibration wafer is used to calibrate both the downward and upward looking microscope cameras. This ceramic wafer has two metal pins that have been bonded into the wafer, perpendicular to the surface. The result is that two small circular holes (147 and 244 microns diameter and 488 microns apart) are visible on both sides of the wafer. Originally, we had planned to use the difference in size of the two holes to determine the orientation of the pair, and the known distance between the holes to determine the microscope magnification. However, we found that it is simpler to use a single hole and move the microscope or the calibration wafer with the AMTI robot in order to determine both the magnification and the orientation of the microscopes with respect to either robot or world coordinates.

The process of calibrating the two microscope cameras is as follows:

1. The calibration wafer is first placed in the center location of the pallet. The downward looking microscope views the pin in the calibration wafer from three non-collinear positions by translating the robot in the x and y directions. The microscope magnification and orientation are determined from the image position of the pin and the measured robot positions.

2. The wafer is carefully picked up and brought over to the upward looking microscope. Again, the robot is translated to three non-collinear positions, and the microscope magnification and orientation are determined for the upward looking microscope.

3. The wafer is next rotated and translated to several positions within the field of view of the upward looking microscope. From the image positions of the pin and the measured robot positions, the position of the upward looking microscope in world coordinates and the position offset of the pin with respect to the robot tool coordinates are computed.

4. Once the position offset of the pin is known, the position of the downward looking microscope with respect to the robot tool coordinates is computed. This assumes that the wafer did not shift in the x or y directions when the robot picked it up.

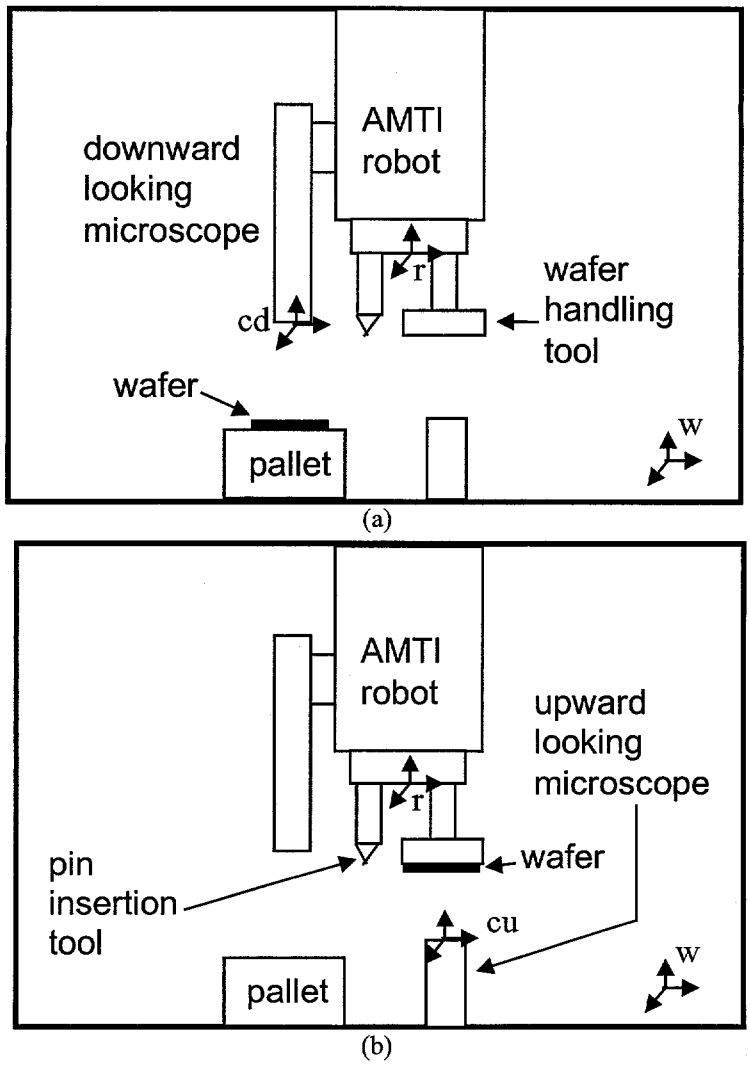

Figure 4 (a) Calibration wafer being viewed by the downward looking microscope. (b) Calibration wafer being viewed by the upward looking microscope.

Figure 4 illustrates a schematic of the workcell and the coordinate frames that describe the position and orientation of the various components. Homogeneous transformations are used to describe the relative positions and orientations between components. The transformations are:

${}^{w}\mathbf{T}_{r}$ = Position and orientation of the robot tool plate with respect to the world;

${}^{w}\mathbf{T}_{rxyz}$ = Position (excluding orientation) of the robot tool plate with respect to the world;

${}^{rxyz}\mathbf{T}_{cd}$ = Position and orientation of the downward looking microscope camera with respect to the robot position;

${}^{w}\mathbf{T}_{cu}$ = Position and orientation of upward looking microscope camera with respect to the world.

When the downward looking microscope is viewing the calibration wafer in the pallet, the position of a feature f (the calibration pin) with respect to the downward camera is related to the same position with respect to the world by

$$ {}^{w}\mathbf{p}_f = {}^{w}\mathbf{T}_{rxyz}\,{}^{rxyz}\mathbf{T}_{cd}\,{}^{cd}\mathbf{p}_f \ . \tag{1} $$

where ${}^{w}\mathbf{p}_f$ is the position of feature f with respect to the world, and ${}^{cd}\mathbf{p}_f$ is the position of feature f with respect to downward looking camera.

When the upward looking microscope is viewing the calibration wafer while the robot is holding it, the position of the feature with respect to the upward looking camera is related to the same position with respect to the robot by

$$ {}^{w}\mathbf{T}_r\,{}^{r}\mathbf{p}_f = {}^{w}\mathbf{T}_{cu}\,{}^{cu}\mathbf{p}_f \ . \tag{2} $$

where ${}^{r}\mathbf{p}_f$ is the position and orientation of feature f with respect to the robot tool plate, and ${}^{cu}\mathbf{p}_f$ is the position of feature f with respect to the upward looking camera.

In addition, the following transformations map 3-D positions into 2-D image coordinates:

$$ {}^{Icd}\mathbf{p}_f = \mathbf{S}_{cd}\,{}^{cd}\mathbf{p}_f \tag{3} $$

$$ {}^{Icu}\mathbf{p}_f = \mathbf{S}_{cu}\,{}^{cu}\mathbf{p}_f \tag{4} $$

where ${}^{Icd}\mathbf{p}_f$ and ${}^{Icu}\mathbf{p}_f$ are the positions of the feature in image coordinates, and $\mathbf{S}_{cd}$ and $\mathbf{S}_{cu}$ are the perspective transformations of the downward and upward looking cameras.

In these equations, ${}^{w}\mathbf{T}_{rxyz}$ and ${}^{w}\mathbf{T}_r$ are the measured positions of the robot, and ${}^{Icd}\mathbf{p}_f$ and ${}^{Icu}\mathbf{p}_f$ are the measured positions of the feature from the downward and upward looking microscopes. The objective of the calibration process is to find the transformations ${}^{rxyz}\mathbf{T}_{cd}$, ${}^{w}\mathbf{T}_{cu}$, $\mathbf{S}_{cd}$, and $\mathbf{S}_{cu}$.

These transformations can be simplified from the normal 6-dimensional representation to a 3-dimensional representation if the following assumptions hold:

A1. Since the AMTI robot is a 4 degree-of-freedom system, all assembly operations are constrained to (x,y,z) translation and rotation about the z axis.

A2. Within the field of view of the downward and upward looking microscopes, the short depth of field constrains the z dimension to be a constant.

Therefore, within the field of view of the microscopes, the transformations are constrained to x and y translation and rotation about the z-axis.

First, let us consider step number one of the calibration process. The downward looking microscope camera, *cd*, is rigidly attached to the x,y,z translation stage of the AMTI robot. Orienting the fourth axis does not effect the position of the downward looking microscope. The position of the hole on the wafer with respect to the world coordinates (${}^{w}x$, ${}^{w}y$) is related to the same position with respect to the camera (${}^{cd}x$, ${}^{cd}y$) by

$$\begin{bmatrix} {}^{w}x \\ {}^{w}y \\ 1 \end{bmatrix} = \begin{bmatrix} 1 & 0 & {}^{w}x_r \\ 0 & 1 & {}^{w}y_r \\ 0 & 0 & 1 \end{bmatrix} \begin{bmatrix} \cos\alpha & -\sin\alpha & {}^{rxyz}x_{cd} \\ \sin\alpha & \cos\alpha & {}^{rxyz}y_{cd} \\ 0 & 0 & 1 \end{bmatrix} \begin{bmatrix} {}^{cd}x \\ {}^{cd}y \\ 1 \end{bmatrix} \tag{5}$$

where $({}^{w}x_r, {}^{w}y_r)$ is the position of the robot tool with respect to the world coordinates, $({}^{rxyz}x_{cd}, {}^{rxyz}y_{cd})$ is the position of the downward looking camera with respect to the robot tool (without orientation about z), and α is the orientation of the camera about z with respect to the robot tool (without orientation about z).

The microscope scales the position of the hole with respect to the downward looking camera by

$$\begin{bmatrix} {}^{Icd}x \\ {}^{Icd}y \\ 1 \end{bmatrix} = \begin{bmatrix} m_{xcd} & 0 & 0 \\ 0 & m_{ycd} & 0 \\ 0 & 0 & 1 \end{bmatrix} \begin{bmatrix} {}^{cd}x \\ {}^{cd}y \\ 1 \end{bmatrix} \tag{6}$$

where $({}^{Icd}x, {}^{Icd}y)$ is the position of the hole in pixels, and (m_{xcd}, m_{ycd}) are the x,y microscope magnification factors.

Combining Equations (5) and (6),

$$\begin{bmatrix} {}^{Icd}x \\ {}^{Icd}y \end{bmatrix} = \begin{bmatrix} m_{xcd} & 0 \\ 0 & m_{ycd} \end{bmatrix} \begin{bmatrix} \cos\alpha & \sin\alpha \\ -\sin\alpha & \cos\alpha \end{bmatrix} \left\{ \begin{bmatrix} {}^{w}x \\ {}^{w}y \end{bmatrix} - \begin{bmatrix} {}^{w}x_r \\ {}^{w}y_r \end{bmatrix} - \begin{bmatrix} {}^{rxyz}x_{cd} \\ {}^{rxyz}y_{cd} \end{bmatrix} \right\} \tag{7}$$

Since the x,y positioning repeatability of the AMTI robot is 0.4 microns, we assume that the robot's position is exact and is known. Also, we are able to measure the position of the hole in image coordinates $({}^{Icd}x, {}^{Icd}y)$. However, the microscope magnification (m_{xcd}, m_{ycd}), the position and orientation of the camera with respect to the robot tool $({}^{rxyz}x_{cd}, {}^{rxyz}y_{cd}, \alpha)$, and the position of the hole with respect to the world coordinates $({}^{w}x, {}^{w}y)$ are not known.

By moving the robot and downward looking camera to three non-collinear positions and recording the location of the hole in image coordinates, we can determine the microscope magnification and orientation of the camera. Since $({}^{rxyz}x_{cd}, {}^{rxyz}y_{cd})$ and $({}^{w}x, {}^{w}y)$ are constant,

$$\begin{bmatrix} ({}^{Icd}x_2 - {}^{Icd}x_1) & ({}^{Icd}x_3 - {}^{Icd}x_2) \\ ({}^{Icd}y_2 - {}^{Icd}y_1) & ({}^{Icd}y_3 - {}^{Icd}y_2) \end{bmatrix} = \begin{bmatrix} m_{xcd}\cos\alpha & m_{ycd}\sin\alpha \\ -m_{ycd}\sin\alpha & m_{xcd}\cos\alpha \end{bmatrix} \begin{bmatrix} ({}^{w}x_{r2} - {}^{w}x_{r1}) & ({}^{w}x_{r3} - {}^{w}x_{r2}) \\ ({}^{w}y_{r2} - {}^{w}y_{r1}) & ({}^{w}y_{r3} - {}^{w}y_{r2}) \end{bmatrix}. \tag{8}$$

In general,

$$\begin{bmatrix} m_{xcd}\cos\alpha & m_{ycd}\sin\alpha \\ -m_{ycd}\sin\alpha & m_{xcd}\cos\alpha \end{bmatrix} = \begin{bmatrix} ({}^{Icd}x_2 - {}^{Icd}x_1) & ({}^{Icd}x_3 - {}^{Icd}x_2) \\ ({}^{Icd}y_2 - {}^{Icd}y_1) & ({}^{Icd}y_3 - {}^{Icd}y_2) \end{bmatrix} \begin{bmatrix} ({}^{w}x_{r2} - {}^{w}x_{r1}) & ({}^{w}x_{r3} - {}^{w}x_{r2}) \\ ({}^{w}y_{r2} - {}^{w}y_{r1}) & ({}^{w}y_{r3} - {}^{w}y_{r2}) \end{bmatrix}^{-1}. \tag{9}$$

Solving for the three unknowns is simplified if the robot moves only in the x direction between points 1 and 2 and then moves only in the y direction between points 2 and 3, i.e. $({}^{w}y_{r2} - {}^{w}y_{r1}) = 0$ and $({}^{w}x_{r3} - {}^{w}x_{r2}) = 0$. Solving for the angle of the camera and the x,y microscope magnification

$$\alpha = \arctan\left(\frac{\left({}^{Icd}y_1 - {}^{Icd}y_2\right) \Big/ \left({}^{w}x_{r2} - {}^{w}x_{r1}\right)}{\left({}^{Icd}y_3 - {}^{Icd}y_2\right) \Big/ \left({}^{w}y_{r3} - {}^{w}y_{r2}\right)} \right), \tag{10}$$

$$m_{xcd} = \frac{\left({}^{Icd}x_3 - {}^{Icd}x_2\right)}{\left({}^{w}y_{r3} - {}^{w}y_{r2}\right)\sin\alpha} \quad \text{and} \quad m_{ycd} = \frac{-\left({}^{Icd}y_2 - {}^{Icd}y_1\right)}{\left({}^{w}x_{r2} - {}^{w}x_{r1}\right)\sin\alpha} \quad \text{if} \quad |\sin\alpha| > 0.01 \ , \tag{11}$$

$$\text{or} \quad m_{xcd} = \frac{\left({}^{Icd}x_2 - {}^{Icd}x_1\right)}{\left({}^{w}x_{r2} - {}^{w}x_{r1}\right)\cos\alpha} \quad \text{and} \quad m_{ycd} = \frac{\left({}^{Icd}y_3 - {}^{Icd}y_2\right)}{\left({}^{w}y_{r3} - {}^{w}y_{r2}\right)\cos\alpha} \quad \text{if} \quad |\sin\alpha| < 0.01 \ . \tag{12}$$

If image noise is a problem, then the robot should be moved to more than 3 points, and a least squares approach [16] should be used to solve for Equation (8). As will be shown in the Experimental Results Section, image noise was not a problem, so a unique solution was adequate.

Similarly, we can solve for the microscope magnification and orientation of the upward looking microscope. In this case, the robot picks up the calibration wafer and the upward looking microscope views the pin from the underside of the wafer. The position of the hole on the wafer with respect to the robot tool $({}^{r}x, {}^{r}y)$ is related to the same position with respect to the upward looking camera $({}^{cu}x, {}^{cu}y)$ by

$$\begin{bmatrix} 1 & 0 & {}^{w}x_r \\ 0 & 1 & {}^{w}y_r \\ 0 & 0 & 1 \end{bmatrix} \begin{bmatrix} {}^{r}x \\ {}^{r}y \\ 1 \end{bmatrix} = \begin{bmatrix} \cos\beta & -\sin\beta & {}^{w}x_{cu} \\ \sin\beta & \cos\beta & {}^{w}y_{cu} \\ 0 & 0 & 1 \end{bmatrix} \begin{bmatrix} {}^{cu}x \\ {}^{cu}y \\ 1 \end{bmatrix} \tag{13}$$

where $({}^{w}x_r, {}^{w}y_r)$ is the position of the robot tool (without orientation about z) with respect to the world coordinates, $({}^{w}x_{cu}, {}^{w}y_{cu})$ is the position of the upward looking camera with respect to the world coordinates, and β is the orientation of the camera about z with respect to the world coordinates. For now, the orientation of the robot tool is assumed to be zero.

The microscope scales the position of the hole with respect to the upward looking camera by

$$\begin{bmatrix} {}^{Icu}x \\ {}^{Icu}y \\ 1 \end{bmatrix} = \begin{bmatrix} m_{xcu} & 0 & 0 \\ 0 & m_{ycu} & 0 \\ 0 & 0 & 1 \end{bmatrix} \begin{bmatrix} {}^{cu}x \\ {}^{cu}y \\ 1 \end{bmatrix} \tag{14}$$

where $({}^{Icu}x, {}^{Icu}y)$ is the position of the hole in pixels, and (m_{xcu}, m_{ycu}) are the x,y microscope magnification factors.

Combining Equations (13) and (14),

$$\begin{bmatrix} {}^{Icu}x \\ {}^{Icu}y \end{bmatrix} = \begin{bmatrix} m_{xcu} & 0 \\ 0 & m_{ycu} \end{bmatrix} \begin{bmatrix} \cos\beta & \sin\beta \\ -\sin\beta & \cos\beta \end{bmatrix} \left\{ \begin{bmatrix} {}^{w}x_r \\ {}^{w}y_r \end{bmatrix} + \begin{bmatrix} {}^{r}x \\ {}^{r}y \end{bmatrix} - \begin{bmatrix} {}^{w}x_{cu} \\ {}^{w}y_{cu} \end{bmatrix} \right\} \ . \tag{15}$$

The position of the hole in image coordinates $({}^{Icu}x, {}^{Icu}y)$ and the robot position $({}^{w}x_r, {}^{w}y_r)$ can be measured. However, the microscope magnification (m_{xcu}, m_{ycu}), the position and orientation of the camera with respect to the world $({}^{w}x_{cu}, {}^{w}y_{cu}, \beta)$, and the position of the hole with respect to the robot tool $({}^{r}x, {}^{r}y)$ are not known.

By moving the robot and the calibration wafer to three non-collinear positions and recording the location of the hole in image coordinates, the microscope magnification and orientation of the camera can be determined. Since $({}^{r}x, {}^{r}y)$ and $({}^{w}x_{cu}, {}^{w}y_{cu})$ are constant,

$$\begin{bmatrix} ({}^{Icu}x_2 - {}^{Icu}x_1) & ({}^{Icu}x_3 - {}^{Icu}x_2) \\ ({}^{Icu}y_2 - {}^{Icu}y_1) & ({}^{Icu}y_3 - {}^{Icu}y_2) \end{bmatrix} = \begin{bmatrix} m_{xcu}\cos\beta & m_{ycu}\sin\beta \\ -m_{ycu}\sin\beta & m_{xcu}\cos\beta \end{bmatrix} \begin{bmatrix} ({}^{w}x_{r2} - {}^{w}x_{r1}) & ({}^{w}x_{r3} - {}^{w}x_{r2}) \\ ({}^{w}y_{r2} - {}^{w}y_{r1}) & ({}^{w}y_{r3} - {}^{w}y_{r2}) \end{bmatrix}. \tag{16}$$

In general,

$$\begin{bmatrix} m_{xcu}\cos\beta & m_{ycu}\sin\beta \\ -m_{ycu}\sin\beta & m_{xcu}\cos\beta \end{bmatrix} = \begin{bmatrix} ({}^{Icu}x_2 - {}^{Icu}x_1) & ({}^{Icu}x_3 - {}^{Icu}x_2) \\ ({}^{Icu}y_2 - {}^{Icu}y_1) & ({}^{Icu}y_3 - {}^{Icu}y_2) \end{bmatrix} \begin{bmatrix} ({}^{w}x_{r2} - {}^{w}x_{r1}) & ({}^{w}x_{r3} - {}^{w}x_{r2}) \\ ({}^{w}y_{r2} - {}^{w}y_{r1}) & ({}^{w}y_{r3} - {}^{w}y_{r2}) \end{bmatrix}^{-1}. \tag{17}$$

Solving for the three unknowns is simplified if the robot moves only in the x direction between points 1 and 2 and then moves only in the y direction between points 2 and 3, i.e. $({}^{w}y_{r2} - {}^{w}y_{r1}) = 0$ and $({}^{w}x_{r3} - {}^{w}x_{r2}) = 0$. Solving for the angle of the camera and the x,y microscope magnification

$$\beta = \arctan\left(\frac{\left({}^{Icu}y_1 - {}^{Icu}y_2\right) \Big/ \left({}^{w}x_{r2} - {}^{w}x_{r1}\right)}{\left({}^{Icu}y_3 - {}^{Icu}y_2\right) \Big/ \left({}^{w}y_{r3} - {}^{w}y_{r2}\right)} \right), \tag{18}$$

$$m_{xcu} = \frac{\left({}^{Icu}x_3 - {}^{Icu}x_2\right)}{\left({}^{w}y_{r3} - {}^{w}y_{r2}\right)\sin\beta} \quad \text{and} \quad m_{ycu} = \frac{-\left({}^{Icu}y_2 - {}^{Icu}y_1\right)}{\left({}^{w}x_{r2} - {}^{w}x_{r1}\right)\sin\beta} \quad \text{if} \quad |\sin\beta| > 0.01, \tag{19}$$

$$\text{or} \quad m_{xcu} = \frac{\left({}^{Icu}x_2 - {}^{Icu}x_1\right)}{\left({}^{w}x_{r2} - {}^{w}x_{r1}\right)\cos\beta} \quad \text{and} \quad m_{ycu} = \frac{\left({}^{Icu}y_3 - {}^{Icu}y_2\right)}{\left({}^{w}y_{r3} - {}^{w}y_{r2}\right)\cos\beta} \quad \text{if} \quad |\sin\beta| < 0.01. \tag{20}$$

Now that the magnification and orientation of each microscope are known, we can go back and determine the position of each microscope. For the upward looking microscope, we are interested in its position with respect to the world coordinates. For the downward looking microscope, we are interested in its position with respect to the robot's tool frame.

Let us begin with the upward looking microscope. To determine its position with respect to the world, we need to find the position of the hole in the calibration wafer with respect to the robot's tool coordinates. This can be accomplished by viewing the hole while rotating the robot's wrist. The set of equations that describe the position of the hole are

$$\begin{bmatrix} \cos\theta & -\sin\theta & {}^{w}x_r \\ \sin\theta & \cos\theta & {}^{w}y_r \\ 0 & 0 & 1 \end{bmatrix} \begin{bmatrix} {}^{r}x \\ {}^{r}y \\ 1 \end{bmatrix} = \begin{bmatrix} \cos\beta & -\sin\beta & {}^{w}x_{cu} \\ \sin\beta & \cos\beta & {}^{w}y_{cu} \\ 0 & 0 & 1 \end{bmatrix} \begin{bmatrix} 1/m_{xcu} & 0 & 0 \\ 0 & 1/m_{ycu} & 0 \\ 0 & 0 & 1 \end{bmatrix} \begin{bmatrix} {}^{Icu}x \\ {}^{Icu}y \\ 1 \end{bmatrix} \tag{21}$$

where θ is the orientation of the robot wrist about the z-axis. From above, we know $(m_{xcu}, m_{ycu}, \beta)$. We can measure the robot position and orientation $({}^{w}x_r, {}^{w}y_r, \theta)$ and the position of the hole in the image plane $({}^{Icu}x, {}^{Icu}y)$. However, we do not know the position of the hole relative to the robot tool frame $({}^{r}x, {}^{r}y)$ or the position of the microscope with respect to the world coordinates $({}^{w}x_{cu}, {}^{w}y_{cu})$. There are two equations and four unknowns. Equation (21) can be written as

$$f_i = \begin{bmatrix} \cos\theta & -\sin\theta & -1 & 0 \\ \sin\theta & \cos\theta & 0 & -1 \end{bmatrix} \begin{bmatrix} {}^{r}x \\ {}^{r}y \\ {}^{w}x_{cu} \\ {}^{w}y_{cu} \end{bmatrix} - \begin{bmatrix} X_i \\ Y_i \end{bmatrix} = 0 \tag{22}$$

where

$$\begin{bmatrix} X_i \\ Y_i \end{bmatrix} = \begin{bmatrix} -{}^{w}x_{ri} + \dfrac{{}^{Icu}x_i}{m_{xcu}}\cos\beta - \dfrac{{}^{Icu}y_i}{m_{ycu}}\sin\beta \\ -{}^{w}y_{ri} + \dfrac{{}^{Icu}x_i}{m_{xcu}}\sin\beta + \dfrac{{}^{Icu}y_i}{m_{ycu}}\cos\beta \end{bmatrix} \tag{23}$$

Moving the hole to $n>2$ points, the least squares problem can be stated as

$$\min_{\Theta} \sum_{i=1}^{n} f_i^T f_i = \min_{\Theta} (A\Theta - b)^T (A\Theta - b) \tag{24}$$

where

$$A = \begin{bmatrix} \cos\theta_1 & -\sin\theta_1 & -1 & 0 \\ \sin\theta_1 & \cos\theta_1 & 0 & -1 \\ \vdots & \vdots & \vdots & \vdots \\ \cos\theta_n & -\sin\theta_n & -1 & 0 \\ \sin\theta_n & \cos\theta_n & 0 & -1 \end{bmatrix}, \quad b = \begin{bmatrix} X_1 \\ Y_1 \\ \vdots \\ X_n \\ Y_n \end{bmatrix}, \quad \text{and} \quad \Theta = \begin{bmatrix} {}^{r}x \\ {}^{r}y \\ {}^{w}x_{cu} \\ {}^{w}y_{cu} \end{bmatrix}.$$

The well-known least squares solution is

$$\Theta = (A^T A)^{-1} A^T b\,. \tag{25}$$

If the robot angle θ_i is not known precisely, an alternative method of locating the position of the upward looking microscope is as follows. First, locate the center of the robot tool in the upward looking camera coordinates, and then add the position of the robot tool with respect to world coordinates. By rotating the robot tool, the hole in the calibration wafer creates an arc in the image coordinates whose center is the robot tool position in camera coordinates. The least squares problem is to

$$\min_{({}^{cu}x_r, {}^{cu}y_r, {}^{cu}r)} \sum_{i=1}^{n} \left[({}^{cu}x_i - {}^{cu}x_r)^2 + ({}^{cu}y_i - {}^{cu}y_r)^2 - ({}^{cu}r)^2 \right]^2 \tag{26}$$

where

$$\begin{bmatrix} {}^{cu}x_i \\ {}^{cu}y_i \\ 1 \end{bmatrix} = \begin{bmatrix} \cos\beta & -\sin\beta & 0 \\ \sin\beta & \cos\beta & 0 \\ 0 & 0 & 1 \end{bmatrix} \begin{bmatrix} 1/m_{xcu} & 0 & 0 \\ 0 & 1/m_{ycu} & 0 \\ 0 & 0 & 1 \end{bmatrix} \begin{bmatrix} {}^{Icu}x_i \\ {}^{Icu}y_i \\ 1 \end{bmatrix}.$$

The location of the upward looking microscope in world coordinates is then

$$\begin{bmatrix} {}^{w}x_{cu} \\ {}^{w}y_{cu} \\ 1 \end{bmatrix} = \begin{bmatrix} {}^{w}x_r \\ {}^{w}y_r \\ 1 \end{bmatrix} - \begin{bmatrix} {}^{cu}x_r \\ {}^{cu}y_r \\ 1 \end{bmatrix} \tag{27}$$

where $({}^{cu}x_r, {}^{cu}y_r)$ is the solution to (26).

The location of the downward looking microscope with respect to the robot coordinate frame is the last unknown. Unfortunately, we can not use the same technique as above. Instead, we must assume that the robot gently picked up the wafer without moving it laterally. As we will see in the Experimental Results Section, this is a good assumption. The absolute position of the hole $({}^{w}x_{hp}, {}^{w}y_{hp})$ when the wafer is on the pallet is

$$\begin{bmatrix} {}^{w}x_{hp} \\ {}^{w}y_{hp} \\ 1 \end{bmatrix} = \begin{bmatrix} \cos\theta_p & -\sin\theta_p & {}^{w}x_{rp} \\ \sin\theta_p & \cos\theta_p & {}^{w}y_{rp} \\ 0 & 0 & 1 \end{bmatrix} \begin{bmatrix} {}^{r}x \\ {}^{r}y \\ 1 \end{bmatrix} \tag{28}$$

where $({}^{r}x, {}^{r}y)$ is the relative position of the hole with respect to the robot wrist as found in Equation (25), and $({}^{w}x_{rp}, {}^{w}y_{rp}, \theta_p)$ are the position and orientation of the robot when the wafer is picked up from the pallet. The position of the downward looking microscope $({}^{rxyz}x_{cd}, {}^{rxyz}y_{cd})$ can be computed as

$$\begin{bmatrix} {}^{rxyz}x_{cd} \\ {}^{rxyz}y_{cd} \\ 1 \end{bmatrix} = \begin{bmatrix} {}^{w}x_{hp} \\ {}^{w}y_{hp} \\ 1 \end{bmatrix} - \begin{bmatrix} 1 & 0 & {}^{w}x_{ri} \\ 0 & 1 & {}^{w}y_{ri} \\ 0 & 0 & 1 \end{bmatrix} \begin{bmatrix} \cos\gamma & -\sin\gamma & 0 \\ \sin\gamma & \cos\gamma & 0 \\ 0 & 0 & 1 \end{bmatrix} \begin{bmatrix} 1/m_{xcd} & 0 & 0 \\ 0 & 1/m_{ycd} & 0 \\ 0 & 0 & 1 \end{bmatrix} \begin{bmatrix} {}^{Icd}x_i \\ {}^{Icd}y_i \\ 1 \end{bmatrix} \tag{29}$$

where $({}^{w}x_{ri}, {}^{w}y_{ri})$ is anyone of the three positions (*i=1,2,or 3*) of the robot when viewing the hole with the downward looking microscope (see Equations (10) to (12)), and $({}^{Icd}x_i, {}^{Icd}y_i)$ is the corresponding position of the hole in the image.

Once calibrated, the vision system can be used to determine the position of pins and gears and the tool offset of the pin insertion tool. For example, the location of a pin or hole $({}^{w}x_{fd}, {}^{w}y_{fd})$ can be determined from the image coordinates of the downward looking microscope by

$$\begin{bmatrix} {}^{w}x_{fd} \\ {}^{w}y_{fd} \\ 1 \end{bmatrix} = \begin{bmatrix} 1 & 0 & {}^{w}x_{rfd} \\ 0 & 1 & {}^{w}y_{rfd} \\ 0 & 0 & 1 \end{bmatrix} \begin{bmatrix} \cos\gamma & -\sin\gamma & {}^{rxyz}x_{cd} \\ \sin\gamma & \cos\gamma & {}^{rxyz}y_{cd} \\ 0 & 0 & 1 \end{bmatrix} \begin{bmatrix} 1/m_{xcd} & 0 & 0 \\ 0 & 1/m_{ycd} & 0 \\ 0 & 0 & 1 \end{bmatrix} \begin{bmatrix} {}^{Icd}x_{fd} \\ {}^{Icd}y_{fd} \\ 1 \end{bmatrix} \tag{30}$$

where $({}^{Icd}x_{fd}, {}^{Icd}y_{fd})$ is the image position of the feature, and $({}^{w}x_{rfd}, {}^{w}y_{rfd})$ is the position of the robot when the image is taken.

Using the upward looking microscope, the position offset of the pin insertion tool is determined from a hole in the center of the tool. Its position offset with respect to the robot wrist $({}^{r}x_{fu}, {}^{r}y_{fu})$ is given by

$$\begin{bmatrix} {}^{r}x_{fu} \\ {}^{r}y_{fu} \\ 1 \end{bmatrix} = \begin{bmatrix} \cos\theta_{fu} & -\sin\theta_{fu} & {}^{w}x_r \\ \sin\theta_{fu} & \cos\theta_{fu} & {}^{w}y_r \\ 0 & 0 & 1 \end{bmatrix}^{-1} \begin{bmatrix} \cos\beta & -\sin\beta & {}^{w}x_{cu} \\ \sin\beta & \cos\beta & {}^{w}y_{cu} \\ 0 & 0 & 1 \end{bmatrix} \begin{bmatrix} 1/m_{xcu} & 0 & 0 \\ 0 & 1/m_{ycu} & 0 \\ 0 & 0 & 1 \end{bmatrix} \begin{bmatrix} {}^{Icu}x_{fu} \\ {}^{Icu}y_{fu} \\ 1 \end{bmatrix} \tag{31}$$

where $({}^{Icu}x_{fu}, {}^{Icu}y_{fu})$ is the image position of the insertion tool and θ_{fu} is the wrist orientation when the image is taken.

Using Equations (30) and (31), the pins can be picked up and inserted, and the gears and pins can be aligned. For example, when picking up a pin, the *x,y* position of the robot is determined by solving

$$\begin{bmatrix} {}^{w}x_{fd} \\ {}^{w}y_{fd} \\ 1 \end{bmatrix} = \begin{bmatrix} \cos\theta & -\sin\theta & {}^{w}x_{r} \\ \sin\theta & \cos\theta & {}^{w}y_{r} \\ 0 & 0 & 1 \end{bmatrix} \begin{bmatrix} {}^{r}x_{fu} \\ {}^{r}y_{fu} \\ 1 \end{bmatrix} \tag{32}$$

for $({}^{w}x_{r}, {}^{w}y_{r})$ where θ is any arbitrary robot wrist angle, and $({}^{w}x_{fd}, {}^{w}y_{fd})$ and $({}^{r}x_{fu}, {}^{r}y_{fu})$ are the locations of the pin and pin insertion tool as given in Equations (30) and (31). When placing the wafer of gears on the press-fit pins, the x,y position and orientation of the robot are determined by solving

$$\begin{bmatrix} \cos\lambda & -\sin\lambda & {}^{w}x_{fd1} \\ \sin\lambda & \cos\lambda & {}^{w}y_{fd1} \\ 0 & 0 & 1 \end{bmatrix} = \begin{bmatrix} \cos\theta & -\sin\theta & {}^{w}x_{r} \\ \sin\theta & \cos\theta & {}^{w}y_{r} \\ 0 & 0 & 1 \end{bmatrix} \begin{bmatrix} \cos\gamma & -\sin\gamma & {}^{r}x_{fu1} \\ \sin\gamma & \cos\gamma & {}^{r}y_{fu1} \\ 0 & 0 & 1 \end{bmatrix} \tag{33}$$

for $({}^{w}x_{r}, {}^{w}y_{r}, \theta)$. The locations of pins 1 and 2 with respect to the world coordinates are $({}^{w}x_{fd1}, {}^{w}y_{fd1})$ and $({}^{w}x_{fd2}, {}^{w}y_{fd2})$ as given in Equation (30). The locations of gears 1 and 2 with respect to the robot coordinates are $({}^{r}x_{fu1}, {}^{r}y_{fu1})$ and $({}^{r}x_{fu2}, {}^{r}y_{fu2})$ as given in Equation (31). The orientations of the pins and gears are given by

$$\lambda = \arctan\left(\frac{{}^{w}y_{fd2} - {}^{w}y_{fd1}}{{}^{w}x_{fd2} - {}^{w}x_{fd1}}\right) \quad \text{and} \quad \gamma = \arctan\left(\frac{{}^{r}y_{fu2} - {}^{r}y_{fu1}}{{}^{r}x_{fu2} - {}^{r}x_{fu1}}\right). \tag{34}$$

Experimental Results

The calibration procedure was executed several times to quantify the variability of the procedure. Tables 1 to 3 show the results of these tests. From Table 1, the resolution of the downward looking camera is approximately 5.9 microns/pixel, while the resolution of the upward looking camera is approximately 4.8 microns/pixel. However, when determining the center location of the holes, a subpixel precision of 3.3 microns (3 standard deviations -- 3σ) for the downward looking microscope and 1.3 microns (3σ) for the upward looking microscope was typically achieved.

Tables 2 and 3 show that the two methods for determining the upward looking microscope's location produce substantially different results. While the mean error in Table 2 is extremely low, the standard deviation (root mean squared error) shows that errors in the fit data can reach up to 68 microns (3σ). On the other hand, the standard deviation in Table 3 shows that errors in the fit data are typically less than 3.6 microns (3σ). These results lead us to conclude that the resolution of the wrist angle used in the calculations is not accurate enough. Although the wrist motor has a repeatability of 0.006 degrees, the belt between the motor and the wrist axis allows for considerable errors. In fact, we estimate the wrist errors to be up to 0.1 degrees over a 10 degree rotation, based on the circular fit using Equation (26). Therefore, the least squares fit using Equation (26) is used for calibration throughout the rest of the tests.

Because of possible errors in wrist orientation, we must also be careful when aligning rows of gears to rows of pins. Instead of applying Equations (33) and (34) only once, it is applied several times, allowing the visual feedback to correct for the wrist orientation error. In the future, we plan to add an additional encoder on the wrist axis to eliminate this orientation error.

To assess the accuracy of the calibration parameters in Table 1 and 3, another test was perform that compared the calculated location of the calibration pin before and after the robot picked up the wafer. First, the downward looking microscope viewed the calibration wafer while it was in the pallet, and the absolute position of the pin was computed. Next, the robot picked up the calibration wafer and translated it over the upward looking camera. The new absolute position of the calibration pin was computed from the upward looking microscope image coordinates. This position was compared to the translated position computed from the downward looking microscope. This test was repeated 10 times. Table 4 shows that

the repeatability was 1.3 microns with a standard deviation of 0.5 microns. This error includes vision calibration errors as well as a possible displacement of the wafer when it is being picked up. Since the clearance holes of the gears are 8-11 microns larger than the pin diameters, these calibration results were concluded to be accurate enough to perform the gear placement task. If necessary, better resolution could be achieved by increasing the magnification of the microscopes, which are currently at their lowest setting.

Table 1. Vision calibration parameters for 10 trials.

	Mean (pixels/mm)	Standard Deviation
m_{xcd}	171.9016 pixels/mm	0.18960 pixels/mm
m_{ycd}	173.4098 pixels/mm	0.13797 pixels/mm
α	-88.5810 degrees	0.01933 degrees
m_{xcu}	-208.7504 pixels/mm	0.09288 pixels/mm
m_{ycu}	209.3141 pixels/mm	0.04987 pixels/mm
β	-92.6970 degrees	0.04705 pixels/mm

Table 2. Vision calibration parameters derived from fitting 9 data points using Equation (25).

${}^{r}x$	20.6575 mm
${}^{r}y$	22.9962 mm
Mean error from data point	2.8816×10^{-14} mm
Standard deviation from data point	0.0227 mm
${}^{w}x_{cu}$	125.0708 mm
${}^{w}y_{cu}$	8.7608 mm
${}^{rxyz}x_{cd}$	2.9427 mm
${}^{rxyz}y_{cd}$	109.6385 mm

Table 3. Vision calibration parameters derived from fitting 9 data points using Equation (26). Matlab's LEASTSQ routine was used to solve the circular least squares fit.

${}^{cu}x_{r}$	21.3728 mm
${}^{cu}y_{r}$	24.8062 mm
${}^{cu}r$	31.1236 mm
Mean error from circular fit	-2.0×10^{-8} mm
Standard deviation from circular fit	0.0012 mm
${}^{w}x_{cu}$	125.0496 mm
${}^{w}y_{cu}$	8.5336 mm
${}^{rxyz}x_{cd}$	2.9254 mm
${}^{rxyz}y_{cd}$	109.4062 mm

Table 4. Location errors of the calibration pin when viewed before and after the robot picked up the wafer.

	Mean	Standard Deviation
e_x	0.1040 microns	0.3523 microns
e_y	1.2526 microns	0.5365 microns
$\sqrt{e_x^2 + e_y^2}$	1.3106 microns	0.5088 microns

Once the vision system is calibrated, the assembly process is as follows.

1. The upward looking microscope locates the center of the pin insertion tool with respect to the robot tool frame using Equation (31).
2. The downward looking microscope locates a pin in the left most wafer (the one with the clearance holes) using Equation (30).
3. The pin insertion tool is moved just above the pin using Equation (32). The downward pneumatic valve of the insertion tool is activated, pushing the tool over the pin. A vacuum is applied to the tool tip, picking up the pin. The upward value of the insertion tool is activated, lifting the tool.
4. The downward looking microscope locates a hole in the middle wafer (the one with press-fit holes) using Equation (30).
5. The pin insertion tool with the pin is moved just above the hole using Equation (32). The downward valve of the insertion tool is activated, pressing the pin into the hole. The vacuum at the tool tip is released, and the upward valve of the insertion tool is activated, thus lifting the tool and leaving the press-fit pin.
6. Steps 2 through 5 are repeated for several pins.
7. The downward looking microscope locates two pins in the middle wafer using Equation (30). The orientation of the rows of pins is determined from these two positions from Equation (34).
8. The vacuum chuck tool picks up the right wafer (the one with the gears) and positions it over the upward looking microscope.
9. The upward looking microscope locates the center of two gears with respect to the robot tool frame using Equation (31). The orientation of the rows of gears is determined from these two positions from Equation (34). The robot wrist is rotated to align the orientation of the rows of gears to the rows of pins. Because of possible wrist rotation error, this step is repeated several times until an acceptable error is reached.
10. The robot places the wafer of gears over the wafer of pins using Equation (33).

Figure 5 shows the robot picking up a 386-micron diameter pin. Figures 6 and 7 show the robot placing the wafer of gears over the wafer of pins. These experiments were repeated several times, and as long as the vision system correctly located a pin or hole, it never failed. In those cases where the vision system failed to locate a pin or hole, it was typically because of scratches or dust that had accumulated around the hole. At the time of publication, the gears have not been released from a top wafer. However, a close visual inspection from the side of the wafer shows that the gears are being placed on the pins. This is verified by the contact between the surface of the two wafers, and the fact that they do not slip laterally.

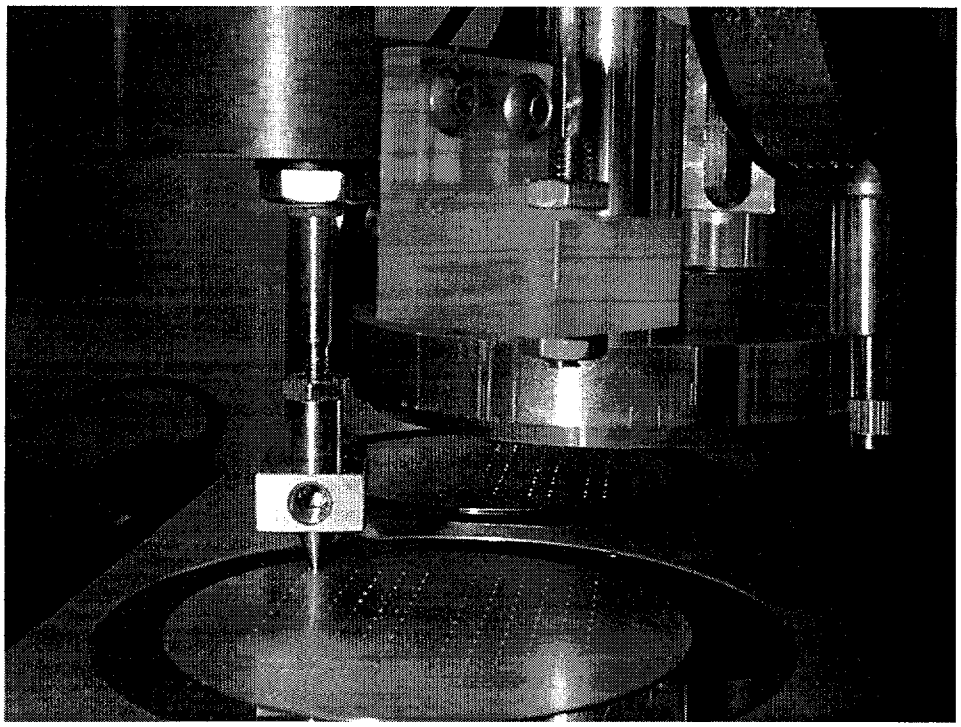

Figure 5. The pin insertion tool is picking up a 386-micron diameter pin. The pin is placed in the wafer in the background.

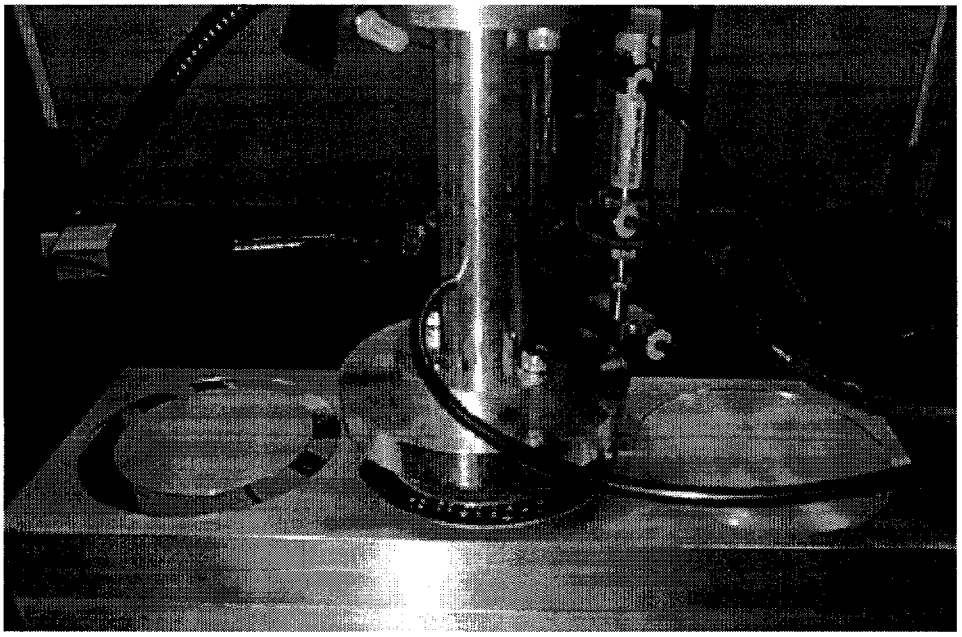

Figure 6. The wafer of gears is being placed on the wafer of pins.

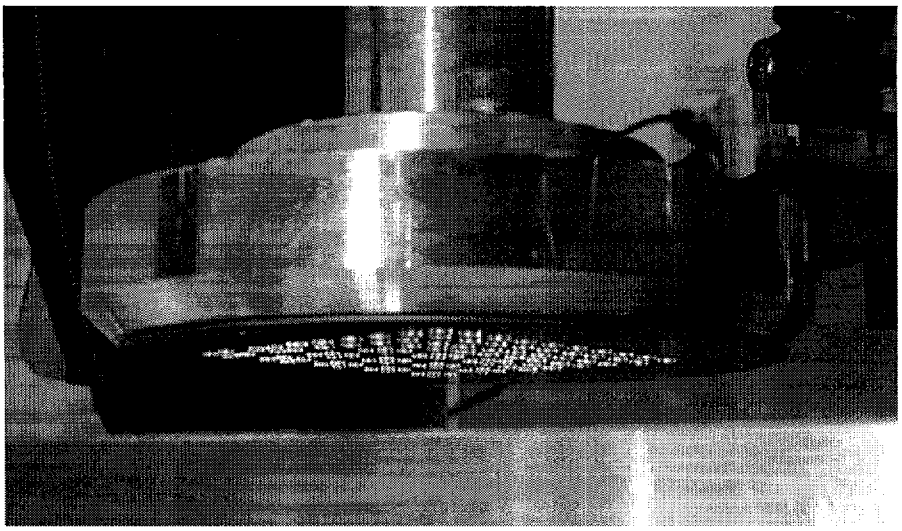

Figure 7. View of the wafer of gears before being placed on the pins.

Conclusion

In this paper, we described a parallel assembly technique for assembling multiple layers of LIGA components into complex structures, such as a geared transmission. The "standard" processes for this parallel assembly would consist of four steps: fabrication, assembly, diffusion bonding, and release. These steps would be repeated several times, each time adding a new layer of LIGA to the final assembly. In this paper, we investigated the assembly step. This step consists of automatically inserting multiple pins into a substrate, and then placing a wafer with multiple gears onto the pins. A dual microscope system was used to locate the pins accurately and align the wafers to within 3 microns. Future work will concentrate on integrating the assembly step with the diffusion bonding and release steps.

Acknowledgements

The authors thank Ron Simon for designing the pallet and wafer-handling tool, David Armor for designing the pin insertion tool, Marc Polosky for designing the calibration wafer, Merlin Decker for designing the pin holder and press-fit wafer, and Andy Jojola for chamfering the pins. We also thank Jim Barr from Vanderbilt University for programming the robot.

References

1. D. Banks, "Introduction to Microengineering," http://www.ee.surrey.ac.uk/Personal/D.Banks/umintro.html.
2. L.Y. Lin, S. S. Lee, K. S. J. Pister, and M. C. Wu, "Micro-machined Three-Dimensional Micro-Optics for Integrated Free-Space Optical System," *IEEE Photonics Technology Letters*, Vol. 6, No. 12, pp. 1445-1447, December 1994.
3. H. Guckel, "Deep X-ray Lithography for Micromechanics via Synchrotron Radiation," *Nuclear Instruments and Methods in Physics Research B79*, pp. 247-248, 1993.
4. H. Guckel, K.J. Skrobis, T.R. Christenson, J. Klein, S. Han, B. Choi, E.G. Lovel, "Fabrication of Assembled Micromechanical Components via Deep X-Ray Lithography," *Proc. IEEE MEMS '91*, Nara, Japan, pp. 74-79, 1991.
5. T. Tanikawa and T. Arai, "Development of a Micro-Manipulation System Having a Two-Fingered Micro-Hand," *IEEE Transactions on Robotics and Automation*, Vol. 15, No. 1, pp. 152-162, February 1999.

6. H. Miyazaki, T. Sato, "Pick and Place Shape Forming of Three-Dimensional Micro Structures from Fine Particles," *Proc. of ICRA 1996*, pp. 2535-2540.
7. W. Zesch, M. Brunner, A. Weber, "Vacuum Tool for Handling Microobjects with a Nanorobot," *Proc. of ICRA 1997*, pp. 1761-1766.
8. J.T. Feddema, R. W. Simon, "CAD-Driven Microassembly and Visual Servoing," *Proceedings of the 1998 IEEE International Conference on Robotics and Automation*, Leuven, Belgium, May 16-20, 1998, pp. 1212-1219.
9. Y. Zhou, B.J. Nelson, B. Vikramaditya, "Fusing Force and Vision Feedback for Micromanipulation," *Proceedings of the 1998 IEEE International Conference on Robotics and Automation*, Leuven, Belgium, May 16-20, 1998, pp. 1220-1225.
10. A. Sulzmann, P. Boillat, J. Jacot, "New Developments in 3D Computer Vision for Microassembly," Microrobotics and Micromanipulation, *Proc. of SPIE*, Vol. 3519, pp. 36-47, Boston, November 1998.
11. S. Fatikow and K. Santa, "Planning and Control of a Microassembly Process in a Flexible Microrobot-based Desktop Station," Microrobotics and Micromanipulation, *Proc. of SPIE*, Vol. 3519, pp. 24-35, Boston, November 1998.
12. T. Kasaya, H. Miyazaki, S. Saito, and T. Sato, "Micro Object handling under SEM by Vision-Based Automatic Control," Microrobotics and Micromanipulation, *Proc. of SPIE*, Vol. 3519, pp. 181-191, Boston, November 1998.
13. M. Schuenemann, et. al., "Manufacturing Concepts and Development Trends in the Industrial Production of Microelectromechanical Systems," Microrobots and Microsystem Fabrication, *Proc. of SPIE*, Vol. 3202, Pittsburgh, 1997.
14. M. Schuenemann, et. al., "Modularized Microelectromechanical Devices as Key Components for Advanced Intelligent Autonomous Sensors and Control Systems," Sensors and Controls for Advanced Manufacturing,, *Proc. of SPIE*, Vol. 3201, Pittsburgh, 1997.
15. T.R. Christenson, and D.T. Schmale, "A Batch Wafer Scale LIGA Assembly and Packaging Techniques via Diffusion Bonding," *IEEE MEMS '99*, Orlando, Jan. 17-21, 1999.
16. H. Zhuang and Z.S. Roth, *Camera-Aided Robot Calibration*, CRC Press, Inc. 1996.